Synchronization Algorithms for UWB Signals

Cecilia Carbonelli, *Member, IEEE,* and Umberto Mengali, *Life Fellow, IEEE*

***Abstract*—This paper is concerned with timing recovery for ultra-wideband communication systems operating in a dense multipath environment. Two timing algorithms are proposed that exploit the samples of the received signal to estimate the start of the individual frames with respect to the receiver's clock (frame timing) and the location of the first frame in each symbol (symbol timing). Channel estimation comes out as a by-product and can be used for coherent matched filter detection. The proposed algorithms require sampling rates on the order of the inverse of the pulse duration. Their performance is assessed by simulating the operation of coherent and differential detectors. Their sensitivity to the sampling rate is discussed, and the effects of the multiple access interference are evaluated.**

***Index Terms*—Channel estimation, correlation receivers, synchronization, ultra-wideband (UWB) communications.**

I. Introduction

In ITS rule-making proposal [1] of April 2002, the Federal Communications Commission (FCC) defined ultra-wideband (UWB) technology as any wireless transmission scheme that occupies a fractional bandwidth of $W/f_c \geq 20\%$, where W is the transmission bandwidth and f_c is the band center frequency or more than 500 MHz of absolute bandwidth. In traditional UWB systems, also known as impulse radios, such large bandwidths are achieved by transmitting trains of pulses of very low power spectral density and ultrashort duration [2]–[4]. Interest in UWB is motivated by several features including: accurate resolution capability, low probability of interception and detection, enhanced capability to penetrate through obstacles, potentially high user capacity, and robustness against multipath [3], [5], [6]. For these reasons, UWB technology is suitable for short-range indoor communications with high-data-rate wireless connectivity [6]–[8] and offers potential applications in high-resolution ranging [9].

To fully exploit these advantages, however, the channel parameters need to be accurately estimated. In an indoor environment, each pulse generates hundreds of echoes [6] that, in principle, can be resolved and combined in a Rake receiver [3], [5], [10] to exploit the rich diversity of the multipath channel. Unfortunately, the implementation of a Rake is complex because of the large number of fingers needed to capture a significant part of the signal energy and the computational load involved in estimating the gains and delays of the paths [11]. The problem is further exacerbated by pulse distortions due to propagation effects (for example, reflections, diffractions, and scattering from surrounding objects [6], [12], [13]). Taking such distortions into account would require estimating the shapes of the individual echoes.

As an alternative to a Rake, a matched filter receiver can be employed in which the incoming waveform is correlated with an estimate of the channel response. With ideal estimation, this receiver is equivalent to a Rake with infinite fingers and perfect knowledge of the channel gains and delays. Its advantage over a Rake is that pulse distortions are immaterial since the only information required is the shape of the overall channel response and not that of the individual echoes.

Differential detection (DD) [14], [15] and transmitted reference (TR) schemes [16]–[19] are simpler to implement as they do not need channel estimation. Assuming pulse-amplitude modulation (PAM) in DD systems, the symbols are differentially encoded, and each received data pulse is correlated with the previous one. Each pulse serves as a template for the next. In TR schemes, instead, a reference pulse is sent prior to each data pulse, and the channel response to the former is exploited as a template for the latter. The mechanism can be improved by averaging the channel responses from several reference pulses [14], [16], [19].

Whatever the receiver architecture, a synchronization circuit must provide accurate information on the arrival times of the incoming pulses. This is a critical issue that poses a serious challenge to the deployment of UWB radios as a viable and competitive wireless technology [20]–[22]. Timing errors as small as fractions of a nanosecond can seriously degrade the system performance [23], [24].

In UWB communications, a single data symbol is associated with several consecutive pulses, each located in its own frame. Multiple access to the channel is made possible by changing the pulse position within a frame according to a user-specific time-hopping code. Timing recovery may be conveniently viewed as a two-part process. The first part consists of estimating the beginning of the individual frames relative to the receiver's clock ticks. This is called frame timing (FT). The second part consists of identifying the first frame of each symbol in the incoming frame stream and is referred to as symbol timing (ST). Previous work on these subjects may be summarized as follows.

References [25]–[27] approached the FT problem by looking for the peak of the correlation between the received waveform and the repetition of a locally generated template of the transmitted pulse. Various search strategies are investigated and compared in terms of mean acquisition time. Some of them are much

Paper approved by M. Z. Win, the Editor for Equalization and Diversity of the IEEE Communications Society. Manuscript received April 23, 2004. This work was supported by the Italian Ministry of Education in the framework of the Project PRIMO, FIRB 2001. This paper was presented in part at the IEEE Globecom Conference, San Francisco, CA, December 2003, and in part at the IEEE Globecom Conference, Dallas, TX, December 2004.

C. Carbonelli is with the Communication Sciences Institute, University of Southern California, Los Angeles, CA 90089 USA (e-mail: carbonel@usc.edu).

U. Mengali is with the Department of Information Engineering, University of Pisa, 56100 Pisa, Italy (e-mail: umberto.mengali@iet.unipi.it).

Digital Object Identifier 10.1109/TCOMM.2005.863728

more efficient than the traditional "linear search," but large room for improvement remains since a single multipath component is captured by the sliding correlator. In an indoor environment, this amounts to exploiting only a small fraction of the received signal power.

The ST scheme in [28] operates in a nondata-aided (NDA) fashion and hinges on the cyclo-stationary nature of the UWB signals. Its main feature is that it requires only frame-rate sampling, as opposed to subpulse sampling needed for channel estimation. The ST algorithm in [29] is data-aided (DA) and exploits properly designed training sequences. It involves simple integrate-and-dump operations and has an improved acquisition speed compared to [28]. The channel estimation method developed in [11] has an implicit synchronization capability in that it estimates delays (and gains) of the individual multipath components relative to the receiver's time reference. In other words, it recovers both FT and ST and provides an estimate of the channel response. The solution is based on maximum-likelihood (ML) methods and involves subpulse sampling (in the gigahertz range). Approximate ML techniques are adopted in [30] to address the ST problem. They involve low sampling rates (ten times the frame rate or so) and exhibit improved performance compared to [28]. Finally, [31] investigates channel estimation and FT recovery with subspace-based methods. Capitalizing on the concept of innovation rate, the received signal is projected onto a lower dimensional subspace via lowpass/bandpass-filtering and sampling below the Nyquist rate. The timing estimation problem is converted to a harmonic retrieval problem and is solved via a subspace method involving a Vandermonde equation system. The discussion is focused on ranging problems and the goal is limited to the estimation of the propagation delay of the direct path. Extending this method to communications applications with hundreds of paths is problematic and is not pursued. Concerns arise about the implementation complexity and the fact that Vandermonde systems are ill-conditioned if the delays are too closely spaced.

In this study, we investigate both FT and ST. Channel estimation is viewed as a by-product, which can be exploited or not, depending on the detection scheme (coherent or differential). With a pulse duration of 1 ns, it is shown that accurate timing is achieved with sampling rates of around 1 GHz. However, higher rates are needed to achieve satisfactory channel estimates. It is worth noting that our algorithm recovers both FT and ST while those in [28]–[30] are only concerned with ST.

We concentrate on two timing schemes based on least squares (LS) methods. Essentially, they look for the minimum of the Euclidean distance between the received samples and a local replica of their noiseless components. In the first strategy (which is taken from [32]), the FT is recovered first. To do so, a periodic pulse sequence with (frame) period is used and the minimization produces a joint estimate of the channel response and the start of each frame. Subsequently, a training sequence is transmitted and the first frame of each symbol is identified making use of the previous channel and FT estimates. In the second strategy [33], the training sequence is transmitted from the beginning and the minimization leads to channel estimation and FT/ST recovery. The two strategies have comparable performance but different complexity. This study investigates both of them since they are suitable for different operating environments. The first is simpler but it requires that the periodic sequence be transmitted by a single user at a time. The second is more complex but does not put restrictions on the channel access scheme. Both are robust against moderate timing errors and are unaffected by propagation pulse distortions.

This paper is organized as follows. Section II provides the signal model and introduces basic notations. Section III describes the first strategy and Section IV the second. Simulations are discussed in Section V, and conclusions are drawn in Section VI.

II. Signal Model

The transmitted signal is expressed as

$$s(t) = \sum_i a_i \sum_{j=0}^{N_f-1} g(t - iN_fT_f - jT_f - c_jT_c) \qquad (1)$$

where $\{a_i\}$'s are information symbols taking values ± 1 with equal probability, $g(t)$ is the elementary pulse (referred to as *monocycle*), N_f is the number of frames per symbol, T_f is the frame period, T_c is the chip period, and $\{c_j\}_{j=0}^{N_f-1}$ is the time-hopping sequence whose elements are integer values randomly chosen in the range $0 \le c_j \le N_{\rm TH} - 1$.

The channel model we consider is quite general and takes into account propagation effects such as reflections, refractions, and scattering from the objects within the medium. These effects are frequency-sensitive [6], [12], [13] and produce path-dependent distortions on the received pulses. Thus, the channel response to a single pulse $g(t)$ takes the form

$$c(t) = \sum_{l=1}^{N_p} \gamma_l g_l(t - \tau_l) \qquad (2)$$

where $g_l(t)$ is the pulse received from the lth path, γ_l and τ_l are the gain and delay associated with the path, and N_p is the number of paths. The overall waveform resulting from the transmission of $s(t)$ may be written as

$$r(t) = \sum_i a_i \sum_{j=0}^{N_f-1} \sum_{l=1}^{N_p} \gamma_l g_l(t - iN_fT_f - jT_f - \nu T_f - c_jT_c - \tau_l) + w(t). \qquad (3)$$

In this equation, $\nu \in [0, N_f - 1]$ is an integer reflecting the hopping-code misalignment between the transmitter and the receiver in a scale of multiples of T_f, and $w(t)$ is a mixture of Gaussian noise and multiple-access interference (MAI). Without loss of generality, we assume that the minimum path delay $\tau_{\min} = \min_l\{\tau_l\}$ is smaller than the frame duration T_f. Indeed, if it were larger, say, a multiple of T_f plus a fraction, then the multiple part could be absorbed into the code misalignment νT_f.

The received waveform is passed through a filter $g_R(t)$ and is sampled with period $T_s = T_f/Q$, which is a submultiple of

T_f. Integer Q represents the number of samples per frame. The filter output is

$$x(t) = \sum_i a_i \sum_{j=0}^{N_f-1} \sum_{l=1}^{N_p} \gamma_l g'_l(t - iN_fT_f - jT_f - \nu T_f - c_jT_c - \tau_l) + n(t) \quad (4)$$

where $g'_l(t)$ is the convolution $g_l(t) \otimes g_R(t)$ and $n(t)$ represents the filtered noise. This equation may be rewritten in a more convenient form calling μ the integer part of $\tau_{\min}/T_s$ and letting

$$\varepsilon_l = \tau_l - \mu T_s. \quad (5)$$

Note that μ takes values in the range $0 \le \mu \le Q-1$ since $\tau_{\min} < T_f$ by assumption. Substituting (5) into (4) and rearranging yields

$$x(t) = \sum_i a_i \sum_{j=0}^{N_f-1} h(t - iN_fT_f - jT_f - \nu T_f - c_jT_c - \mu T_s) + n(t) \quad (6)$$

with

$$h(t) \doteq \sum_{l=1}^{N_p} \gamma_l g'_l(t - \varepsilon_l). \quad (7)$$

Function $h(t)$ represents the channel response to a monocycle applied at $t = -\mu T_s$ and, in the sequel, is referred to as the *channel response* (CR). Note that the signal component in (6) corresponding to symbol a_k is

$$s_k(t) = a_k \sum_{j=0}^{N_f-1} h(t - kN_fT_f - jT_f - \nu T_f - c_jT_c - \mu T_s). \quad (8)$$

Thus, matched-filter detection requires knowledge of $h(t)$, ν, and μ. Parameter ν identifies the first frame of $s_k(t)$ (beginning at $t = kN_fT_f + \nu T_f$), while μ indicates the frames' starting times (at $t = mT_f + \mu T_f$ with $m = 0, 1, 2, \ldots$). Thus, ST amounts to estimating ν while FT means estimating μ. In the following, we discuss two estimation strategies for $h(t)$, ν, and μ.

Before proceeding, we think it useful to remark on the channel estimation perspective we are taking here. It is clear from (6) that such a perspective subsumes any possible pulse distortion from the channel. In other words, we do not care about distortions because we look for the overall channel response rather than its individual components. This may be called an "unstructured" approach, to contrast it against a "structured" one in which the received pulses all have the same shape, known at the receiver, and the problem reduces to estimating path gains and delays [10], [11]. The structured approach overlooks the propagation physics and does not reflect the experimental evidence that, in UWB channels, the received signal often bears little resemblance to the signal driving the transmit antenna [6], [12], [13].

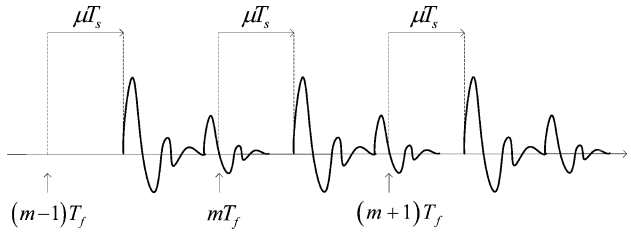

Fig. 1. Noise-free component of the received waveform with no modulation.

III. First Strategy

Assume that $h(t)$ is concentrated on the interval $[0, LT_s)$ and call $h[n] = h(nT_s)$ its samples at multiple of T_s. Letting $\mathbf{h} \doteq [h[0], h[1], \ldots, h[L-1]]^T$ be the sampled version of the CR, in the first strategy, the estimation is carried out in two phases. First, $\mathbf{h}$ and μ are estimated by transmitting a periodic signal of period T_f [this corresponds to setting $a_i \equiv 1$ and $c_j \equiv 0$ in (1)]. Subsequently, the signal is modulated with a training sequence and ν is computed exploiting the previous estimates. We assume that there is no interframe interference, meaning that the channel responses from different monocycles are not overlapped. This requires that T_f exceeds the channel delay spread LT_s plus the maximum difference between consecutive time shifts of the hopping code. Such an assumption greatly simplifies the analysis and allows us to focus on the fundamental aspects of the UWB signal acquisition.

The received waveform in the first phase is

$$x(t) = \sum_j h(t - jT_f - \mu T_s) + n(t). \quad (9)$$

Fig. 1 illustrates the periodic nature of the noise-free component of $x(t)$. In a given frame, the summation in (9) consists of two parts: the truncated CR originating in the current frame and the tail of the CR from the previous frame. The latter is the missing part of the former and vanishes if $T_f - \mu T_s$ exceeds LT_s. Now, suppose that $x(t)$ is observed over M'_f frames and is sampled at $t = mT_f + nT_s$, with $m = 0, 1, \ldots, M'_f - 1$ and $n = 0, 1, \ldots, Q-1$. Letting $x_m[n] \doteq x(mT_f + nT_s)$ and collecting the samples from the mth frame into $\mathbf{x}_m \doteq [x_m[0], x_m[1], \ldots, x_m[Q-1]]^T$, the noise-free components of $\mathbf{x}_m$ may be represented as follows. Denote $\mathbf{p}$ by the Q-dimensional vector obtained by extending $\mathbf{h}$ with $Q-L$ zeroes

$$\mathbf{p} \doteq [h[0], h[1], \ldots, h[L-1], \underbrace{0, 0, \ldots, 0}_{Q-L}]^T \quad (10)$$

and call $\mathbf{v}^{(\downarrow)}[\mu, \mathbf{h}]$ the vector resulting from downshifting the components of $\mathbf{p}$ by μ steps and zero-padding the empty places

$$\mathbf{v}^{(\downarrow)}[\mu, \mathbf{h}] \doteq [\underbrace{0, 0, \ldots, 0}_{\mu}, h[0], h[1], \ldots, h[Q-\mu-1]]^T. \quad (11)$$

It is easily seen that $\mathbf{v}^{(\downarrow)}[\mu, \mathbf{h}]$ represents the (truncated) response originated in the mth frame. Similarly, let $\mathbf{v}^{(\uparrow)}[\mu, \mathbf{h}]$ be

the Q-dimensional vector resulting by up-shifting the components of $\mathbf{p}$ by μ steps and zero-padding the empty places

$$\mathbf{v}^{(\uparrow)}[\mu,\mathbf{h}] \doteq [h[\mu],h[\mu+1],\ldots,h[L-1],\underbrace{0,0,\ldots,0}_{Q-L+\mu}]^T. \quad (12)$$

Clearly, $\mathbf{v}^{(\uparrow)}[Q-\mu,\mathbf{h}]$ represents the tail of the response from the previous frame. Collecting these facts together, we have

$$\mathbf{x}_m = \mathbf{v}^{(\downarrow)}[\mu,\mathbf{h}] + \mathbf{v}^{(\uparrow)}[Q-\mu,\mathbf{h}] + \mathbf{n}_m \quad (13)$$

where $\mathbf{n}_m$ accounts for the noise.

The joint estimation of $\mathbf{h}$ and μ is performed with LS techniques as follows. We seek the values $\tilde{\mu}$ and $\tilde{\mathbf{h}} = [\tilde{h}[0],\tilde{h}[1],\ldots,\tilde{h}[L-1]]$ that minimize the squared Euclidean distance

$$D^2(\tilde{\mu},\tilde{\mathbf{h}}) = \sum_{m=0}^{M_f'-1} \left\| \mathbf{x}_m - \mathbf{v}^{(\downarrow)}[\tilde{\mu},\tilde{\mathbf{h}}] - \mathbf{v}^{(\uparrow)}[Q-\tilde{\mu},\tilde{\mathbf{h}}] \right\|^2. \quad (14)$$

Substituting (11) and (12) into (14) yields

$$D^2(\tilde{\mu},\tilde{\mathbf{h}}) = \sum_{m=0}^{M_f'-1}\sum_{l=0}^{L-1}\left(x_m[|l+\tilde{\mu}|_Q] - \tilde{h}[l]\right)^2 + \sum_{m=0}^{M_f'-1}\sum_{l=L}^{Q-1}\left(x_m[|l+\tilde{\mu}|_Q]\right)^2 \quad (15)$$

where $|l+\tilde{\mu}|_Q$ means $(l+\tilde{\mu})\bmod -Q$. Alternatively, (15) may be written as

$$D^2(\tilde{\mu},\tilde{\mathbf{h}}) = \sum_{m=0}^{M_f'-1}\sum_{l=0}^{Q-1}\left(x_m[|l+\tilde{\mu}|_Q]\right)^2 + M_f'\sum_{l=0}^{L-1}\left(\tilde{h}[l]\right)^2 - 2\sum_{m=0}^{M_f'-1}\sum_{l=0}^{L-1}\tilde{h}[l]x_m[|l+\tilde{\mu}|_Q]. \quad (16)$$

Differentiating with respect to the $\tilde{h}[l]$'s, setting the result to zero, and solving for $\tilde{h}[l]$ yields

$$\tilde{h}[l] = \frac{1}{M_f'}\sum_{m=0}^{M_f'-1} x_m[|l+\tilde{\mu}|_Q], \quad 0\le l\le L-1. \quad (17)$$

Next, substituting (17) into (16) produces

$$D^2(\tilde{\mu},\tilde{\mathbf{h}}) = \sum_{m=0}^{M_f'-1}\sum_{l=0}^{Q-1}\left(x_m[|l+\tilde{\mu}|_Q]\right)^2 - \frac{1}{M_f'}\sum_{l=0}^{L-1}\left(\sum_{m=0}^{M_f'-1} x_m[|l+\tilde{\mu}|_Q]\right)^2. \quad (18)$$

On the other hand, as there are Q samples in a frame, we have

$$\sum_{l=0}^{Q-1}\left(x_m[|l+\tilde{\mu}|_Q]\right)^2 = \sum_{l=0}^{Q-1}(x_m[l])^2 \quad (19)$$

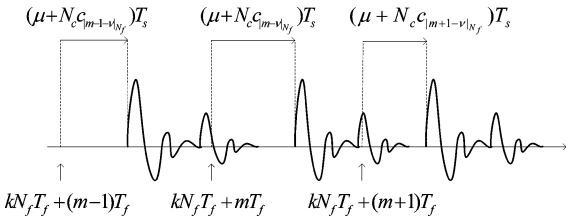

Fig. 2. Noise-free component of the received waveform in the presence of modulation.

which shows that the first term in (18) is independent of $\tilde{\mu}$. Thus, minimizing $D^2(\tilde{\mu},\tilde{\mathbf{h}})$ amounts to maximizing the second term, i.e.,

$$\hat{\mu} = \underset{0\le\tilde{\mu}\le Q-1}{\arg\max}\left\{\sum_{l=0}^{L-1}\left(\sum_{m=0}^{M_f'-1} x_m[|l+\tilde{\mu}|_Q]\right)^2\right\}. \quad (20)$$

Finally, setting $\tilde{\mu}=\hat{\mu}$ in (17) yields the CR estimate

$$\hat{h}[l] = \frac{1}{M_f'}\sum_{m=0}^{M_f'-1} x_m[|l+\hat{\mu}|_Q], \quad 0\le l\le L-1. \quad (21)$$

At this point, we address the estimation of ν, taking advantage of the previous results. In particular, we assume that the transmitted signal is modulated with a training sequence $\{a_i\}$ and the waveform $x(t)$ is observed over K'' symbols ($M_f''=K''N_f$ frames). For simplicity, let $t=0$ be the beginning of the observation interval, and we let $x_{k,m}[n] \doteq x(kN_fT_f+mT_f+nT_s)$. Staking the $x_{k,m}[n]$'s from the m frame $kN_fT_f+mT_f \le t \le kN_fT_f+mT_f+(Q-1)T_s$ into a vector

$$\mathbf{x}_{k,m} \doteq [x_{k,m}[0],x_{k,m}[1],\ldots,x_{k,m}[Q-1]]^T \quad (22)$$

the goal is to estimate $\nu\in[0,N_f-1]$ from the set $\{\mathbf{x}_{k,m}\}$. Fig. 2 shows that, again, in a given frame, the signal component is made of two parts: the truncated channel response originating in the current frame and the tail of the response from the previous frame. Assuming that the chip period T_c is a multiple of T_s, say $T_c=N_cT_s$, and denoting $\lfloor x\rfloor$ the largest relative integer $\le x$, the two parts are $a_{k+\lfloor(m-\nu)/N_f\rfloor}\mathbf{v}^{(\downarrow)}[\mu+N_cc_{|m-\nu|_{N_f}},\mathbf{h}]$ and $a_{k+\lfloor(m-1-\nu)/N_f\rfloor}\mathbf{v}^{(\uparrow)}[Q-\mu-N_cc_{|m-1-\nu|_{N_f}},\mathbf{h}]$, respectively. Correspondingly, we have

$$\mathbf{x}_{k,m} = \mathbf{s}_{k,m}(\mu,\nu,\mathbf{h}) + \mathbf{n}_{k,m} \quad (23)$$

where $\mathbf{n}_{k,m}$ accounts for the noise and

$$\mathbf{s}_{k,m}(\mu,\nu,\mathbf{h}) \doteq a_{k+\lfloor(m-\nu)/N_f\rfloor}\mathbf{v}^{(\downarrow)}[\mu+N_cc_{|m-\nu|_{N_f}},\mathbf{h}] + a_{k+\lfloor(m-1-\nu)/N_f\rfloor}\mathbf{v}^{(\uparrow)}[Q-\mu-N_cc_{|m-1-\nu|_{N_f}},\mathbf{h}]. \quad (24)$$

Replacing μ and $\mathbf{h}$ by $\hat{\mu}$ and $\hat{\mathbf{h}}$ and calling $\tilde{\nu}$ a trial value of ν, the estimate of ν is computed by minimizing

$$D^2(\tilde{\nu},\hat{\mu},\hat{\mathbf{h}}) = \sum_{k=0}^{K''-1}\sum_{m=0}^{N_f-1}\left\|\mathbf{x}_{k,m} - \mathbf{s}_{k,m}(\hat{\mu},\tilde{\nu},\hat{\mathbf{h}})\right\|^2. \quad (25)$$

In the Appendix, an alternative expression of $D^2(\tilde{\nu}, \hat{\mu}, \hat{\mathbf{h}})$ is provided which is more suitable for calculating the minimum.

IV. Second Strategy

In a multiuser scenario, the previous strategy has the drawback that it requires a channel access protocol. Indeed, in the first phase of the estimation, when a periodic signal is transmitted, no other users are allowed to transmit periodic signals as they would interfere with that of the desired user. This limitation is avoided in the second strategy since parameters $\mathbf{h}$, μ, and ν are estimated from a time-hopped signal.

To proceed, we assume that the waveform in (6) is observed over an interval of K symbols and is sampled at $t = kN_fT_f + mT_f + nT_s$, with $k = 0, 1, \ldots, K-1$, $m = 0, 1, \ldots, N_f - 1$, and $n = 0, 1, \ldots, Q-1$. The a_i's are known at the receiver (training sequence). Calling $\tilde{\mathbf{h}}$, $\tilde{\mu}$ and $\tilde{\nu}$ the trial values for $\mathbf{h}$, μ and ν, we aim at minimizing

$$D^2(\tilde{\nu}, \tilde{\mu}, \tilde{\mathbf{h}}) = \sum_{k=0}^{K-1} \sum_{m=0}^{N_f-1} \left\| \mathbf{x}_{k,m} - \mathbf{s}_{k,m}(\tilde{\mu}, \tilde{\nu}, \tilde{\mathbf{h}}) \right\|^2. \quad (26)$$

Letting

$$u[l; a, b] \doteq \begin{cases} 1, & \text{for } a \le l \le b \\ 0, & \text{elsewhere} \end{cases} \quad (27)$$

$$\begin{aligned} z_{k,m}[l; \tilde{\mu}, \tilde{\nu}] \doteq\ & a_{k+\lfloor (m-\nu)/N_f \rfloor} x_{k,m}[l + \tilde{\mu} + N_c c_{|m-\tilde{\nu}|_{N_f}}] \\ & \times u[l; 0, Q - \tilde{\mu} - N_c c_{|m-\tilde{\nu}|_{N_f}} - 1] \\ & + a_{k+\lfloor (m-1-\nu)/N_f \rfloor} x_{k,m} \\ & [l + \tilde{\mu} + N_c c_{|m-1-\tilde{\nu}|_{N_f}} - Q] \\ & \times u[l; Q - \tilde{\mu} - N_c c_{|m-1-\tilde{\nu}|_{N_f}}, L-1] \end{aligned} \quad (28)$$

$$\begin{aligned} M[l; \tilde{\mu}, \tilde{\nu}] \doteq\ & \sum_{k=0}^{K-1} \sum_{m=0}^{N_f-1} [u[l; 0, Q - \tilde{\mu} - N_c\, c_{|m-\tilde{\nu}|_{N_f}} - 1] \\ & + u[l; Q - \tilde{\mu} - N_c\, c_{|m-1-\tilde{\nu}|_{N_f}}, L-1]] \end{aligned} \quad (29)$$

in the Appendix, it is shown that the estimates of $\mathbf{h}$, μ, and ν are

$$(\hat{\mu}, \hat{\nu}) = \underset{(\tilde{\mu}, \tilde{\nu})}{\arg\max} \left\{ \sum_{l=0}^{L-1} \frac{1}{M[l; \tilde{\mu}, \tilde{\nu}]} \left(\sum_{k=0}^{K-1} \sum_{m=0}^{N_f-1} z_{k,m}[l; \tilde{\mu}, \tilde{\nu}] \right)^2 \right\} \quad (30)$$

$$\hat{h}[l] = \frac{1}{M[l; \hat{\mu}, \hat{\nu}]} \sum_{k=0}^{K-1} \sum_{m=0}^{N_f-1} z_{k,m}[l; \hat{\mu}, \hat{\nu}], \quad 0 \leqslant l \leqslant L-1. \quad (31)$$

The following remarks are of interest.

- The second strategy is more complex than the first as it involves the two-dimensional (2-D) search in (30), as opposed to the two one-dimensional (1-D)searches in (20) and (25). Bearing in mind that $0 \le \tilde{\nu} \le N_f - 1$, it is seen that the search in (30) amounts to N_f 1-D searches.
- Both strategies can be used for tracking $\mathbf{h}$, μ, and ν. The need for tracking stems from two different circumstances. On one the one hand, the CR is time varying with the physical environment (for example, people walking in an office area reflect the impinging waves and generate time-varying propagation paths). On the other hand, it arises from imperfect alignment of the transmit/receive clock frequencies. To understand this problem, suppose that the transmitter frame period $T_f^{(T)}$ is slightly different from the receiver frame period $T_f^{(R)}$ (as a consequence of thermal drifts of the oscillators and other impairments). Then, on the receiver time scale (which ticks at multiples of $T_f^{(R)}$), the arriving pulses are seen to drift rightward or leftward depending on whether $T_f^{(R)}$ is greater or smaller than $T_f^{(T)}$. In any case, μ and ν will vary periodically in a saw-tooth fashion in the intervals $0 \le \mu \le Q-1$ and $0 \le \mu \le N_f - 1$.

With the first strategy, the tracking is implemented by repeating the estimation procedure at regular intervals. In doing so, a reduction in the data rate is incurred as no information is transmitted during the synchronization intervals. This drawback is avoided in the second strategy as the estimation procedure may be carried out in a decision-directed mode, i.e., by replacing the training symbols with the detector decisions. In either way, the interval between consecutive updates depends on the detection process. With a correlation detector, the interval must be small compared with the channel decorrelation time such that the drift is within a fraction of the pulse duration. With a differential receiver, and vice versa, the channel variations need only be negligible over a symbol interval, which is normally true in most indoor applications. As for the drift, it must be small compared with the channel delay spread, not the pulse duration. Thus, the time interval between consecutive updates may be much longer than in a correlation detector.

V. Simulation Model and Results

The channel model is that indicated as CM1 by the IEEE 802.15.3a channel modeling subcommittee for use in the evaluation of UWB physical-layer submissions [34]. The channel impulse responses are truncated beyond 60 ns.

A. Signal and Interference

We assume that K_u users are simultaneously active in the environment, each "seeing" its own channel with the statistics described above. Channels of different users are generated independently of each other. The first user is the desired one, and the others are interferers. The signal transmitted by the kth user is modeled as

$$s^{(k)}(t) = \sum_{i=-\infty}^{+\infty} \sum_{j=0}^{N_f-1} a_i^{(k)} g(t - iN_fT_f - jT_f - c_j^{(k)}T_c - \tau^{(k)}) \quad (32)$$

where all of the parameters have an obvious meaning except $\tau^{(k)}$, which accounts for the asynchronism of the users and is uniformly distributed in the range $0 \le \tau^{(k)} \le N_fT_f$. Pulse $g(t)$ is shaped as the second derivative of a Gaussian function and has a width of 1 ns. The frame period T_f is set equal to 100 ns, the number of frames per symbol N_f is 25, the chip period T_c is 2 ns, and the elements $c_j^{(k)}$ of the time-hopping code

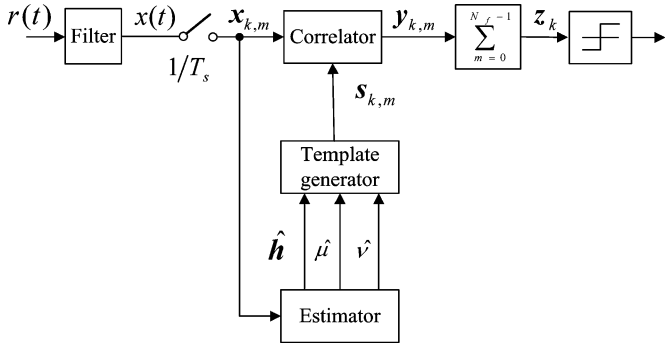

Fig. 3. Block diagram for a coherent receiver.

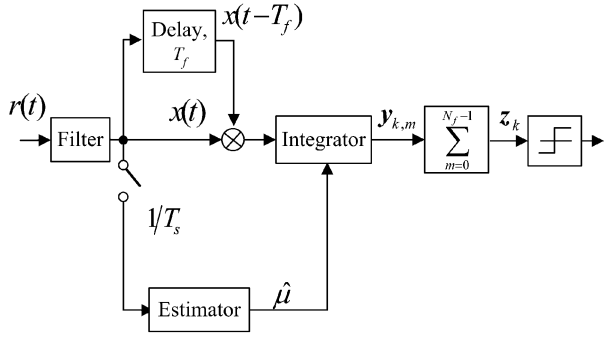

Fig. 4. Block diagram for a differential receiver.

are randomly chosen in the interval $0 \le c_j^{(k)} \le 24$. The receive filter has a rectangular transfer function over ± 4 GHz and the thermal noise is white, with a two-sided spectral density $N_0/2$. The sampling rate Q/T_f is 8 GHz or lower. The Nyquist rate corresponds to $Q = 800$ samples per frame.

The performance of the estimation algorithms is expressed as a function of the SNR and the number of active users. The former is defined as the ratio E_b/N_0, where E_b is the energy per symbol of the desired user's signal at the filter output (before sampling). As the channel responses from different excitation pulses are not overlapped by design, from (6), it is seen that E_b is N_f times the energy of $h(t)$. In the absence of MAI and with perfect channel and timing knowledge, the bit-error rate (BER) of an ideal coherent receiver (ICR) operating on the filter's analog output is

$$P(e) = Q\left(\sqrt{\frac{2E_b}{N_0}}\right) \tag{33}$$

where $Q(x)$ is the standard Q-function. After sampling, the BER of an ICR is still as in (33) except that the signal energy is now

$$E_b^{(\text{samp})} = T_s N_f \sum_{l=0}^{L-1} h^2[l]. \tag{34}$$

It is readily shown that $E_b^{(\text{samp})} = E_b$ for Nyquist sampling, whereas $E_b^{(\text{samp})} < E_b$ for lower sampling rates. Undersampling entails an energy loss and increases the error probability.

B. Coherent and Differential Receivers

The estimation algorithms described above have been applied to coherent and differential receivers [14]–[16]. Fig. 3 illustrates a coherent scheme. Its heart is the correlation unit where, frame by frame, the product $y_{k,m} = \mathbf{x}_{k,m}^T \mathbf{s}_{k,m}(\hat{\mu}, \hat{\nu}, \hat{\mathbf{h}})$ is computed between $\mathbf{x}_{k,m}$ and the local template $\mathbf{s}_{k,m}(\hat{\mu}, \hat{\nu}, \hat{\mathbf{h}})$. The decision statistic is the summation of the $y_{k,m}$'s over the N_f frames of the symbol.

With differential detection, we assume for simplicity that there is no MAI ($K_u = 1$) and a symbol has just one frame ($N_f = 1$). Under these circumstances, the only timing parameter of interest is μ, indicating the beginning of the frames (symbols) relative to the local clock's ticks. There is no time-hopping, which amounts to setting $c_j = 0$ in the formulas. Correspondingly, the quantity in squared brackets in (29) is always unity, and we have $M[l; \tilde{\mu}, \tilde{\nu}] = K$. Also, (28) becomes

$$\begin{aligned} z_k[l; \tilde{\mu}] =& a_k x_k[l + \tilde{\mu}] u[l; 0, Q - \tilde{\mu} - 1] \\ &+ a_{k-1} x_k[l + \tilde{\mu} - Q] u[l; Q - \tilde{\mu}, L - 1] \end{aligned} \tag{35}$$

with $\mathbf{x}_k = [x_k[0], x_k[1], \ldots, x_k[Q-1]]^T$, and (30) and (31) boil down to

$$\hat{\mu} = \underset{0 \le \tilde{\mu} \le Q-1}{\arg\max} \left\{ \sum_{l=0}^{L-1} \left(\sum_{k=0}^{K-1} z_k[l; \tilde{\mu}] \right)^2 \right\} \tag{36}$$

$$\hat{h}[l] = \frac{1}{K} \sum_{k=0}^{K-1} z_k[l; \hat{\mu}], \quad 0 \le l \le L-1. \tag{37}$$

The block diagram of the receiver is shown in Fig. 4. The lower and upper integration limits for the kth symbol are $t_k^{(-)} = kT_f + \hat{\mu}T_s$ and $t_k^{(+)} = t_k^{(+)} + LT_s$.

The channel delay spread L plays an important role in the estimation and detection processes. Its choice is based on the following considerations. In indoor communications, a realistic channel response $h(t)$ contains hundreds of echoes of the original transmitted pulse, with decreasing amplitudes as the differential delays increase relative to the first echo. Therefore, most of channel response energy is concentrated in the initial part of $h(t)$. With the channel model adopted in the simulations, about 90% of the energy is concentrated in the first $\Delta t = 20$ ns of the response. This suggests taking $L = \Delta t/T_s$. With a shorter L, a significant fraction of the energy would be missed while, with a longer L, the tail of $h(t)$ would be poorly estimated. In a coherent receiver, this would worsen the receiver performance as the last elements of the template $\mathbf{s}_{k,m}(\hat{\mu}, \hat{\nu}, \hat{\mathbf{h}})$ would be noisy.

C. Simulation Results

Fig. 5 illustrates the BER performance of a coherent receiver where the parameters μ, ν, and $\mathbf{h}$ are estimated with the two strategies described above. There is a single active user, and the total estimation time T_{est} is 30 symbol intervals. With the first strategy, 25 intervals are allotted to the estimation of μ and $\mathbf{h}$, while the remaining five serve to measure ν. As the two strategies are nearly equivalent, in the sequel, we concentrate on the second.

Fig. 6 shows the BER of coherent receivers operating with various sampling rates. A single user is assumed and $T_{\text{est}} = 50$ symbols. Dashed lines correspond to an ICR (with perfect

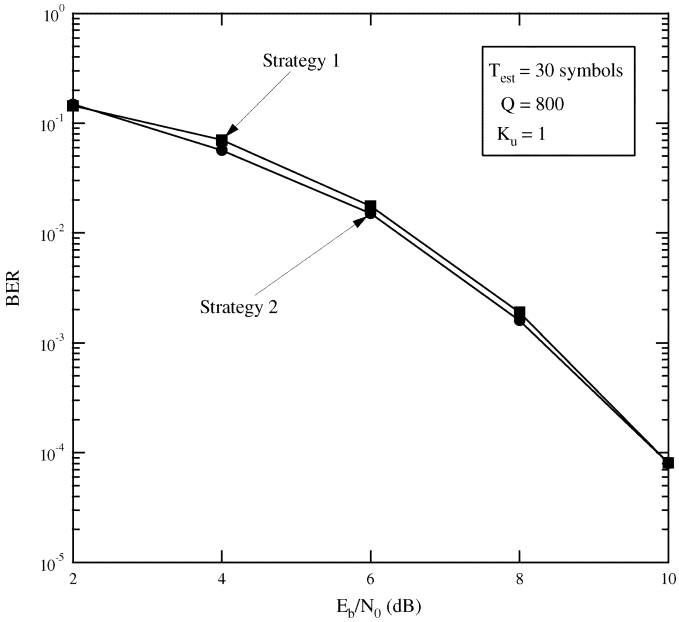

Fig. 5. BER versus E_b/N_0 with the two estimation strategies.

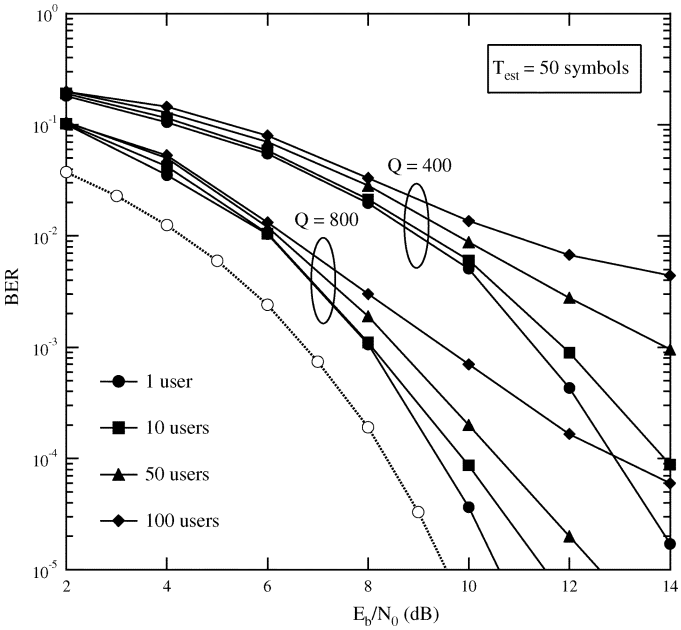

Fig. 7. BER versus E_b/N_0 in the presence of MAI.

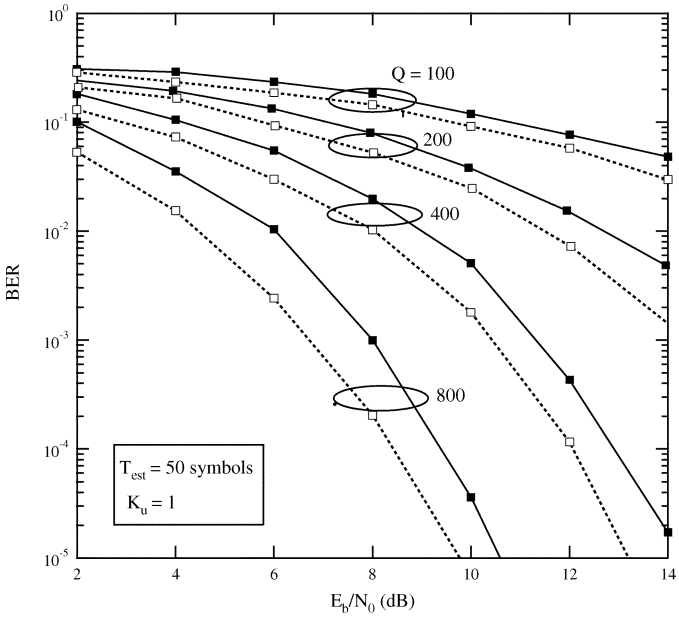

Fig. 6. BER versus E_b/N_0 with different sampling rates.

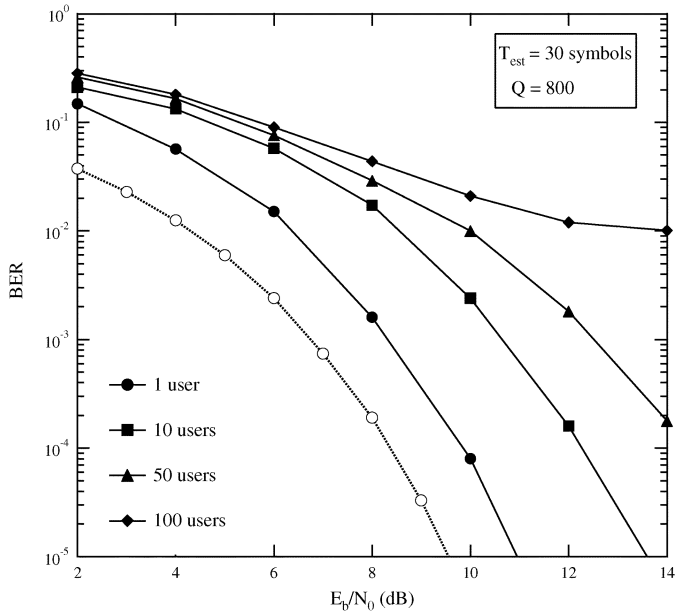

Fig. 8. BER versus E_b/N_0 in the presence of MAI with $T_{\rm est} = 30$.

knowledge of μ, ν, and $\mathbf{h}$) while solid lines take the estimation errors into account. As expected, the performance degrades as the sampling rate decreases. Note that the horizontal distance between solid (dashed) lines with $Q = 800$ and $Q = 400$ is about 3 dB, as is the distance between solid (dashed) lines with $Q = 400$ and $Q = 200$. The physical explanation is that halving the sampling rate amounts to (approximately) halving the signal energy. Even with $Q = 800$ samples per frame, a gap of about 0.8 dB remains between the solid and dashed lines. Further simulations indicate that most of the loss comes from the estimation of $\mathbf{h}$. Indeed, the gap reduces to approximately 0.1–0.2 by replacing $\hat{\mathbf{h}}$ by the true $\mathbf{h}$.

Simulations in the presence of MAI are illustrated in Fig. 7. The receiver is still coherent, Q is either 800 or 400, and the number of users varies from 1 through 100. The dashed line corresponds to an ICR operating with $Q = 800$. The BER degradation as K_u increases results from two separate mechanisms: the growth of the interference at the detector input and the worsening of the synchronization and channel estimation functions. The latter can be alleviated by increasing the estimation time but the improvement is small for $T_{\rm est}$ exceeding 50 symbols or so. Vice versa, significant degradations occur with $T_{\rm est}$ smaller than 50 symbols. This is made clear by the results in Fig. 8 corresponding to $Q = 800$ and $T_{\rm est} = 30$. Comparing with Fig. 7, it is seen that the loss increases with the number of users.

Fig. 9 shows the performance of a differential receiver. The dashed line represents the BER with perfect knowledge of μ, while solid lines account for the timing errors. For $E_b/N_0 \gg 1$,

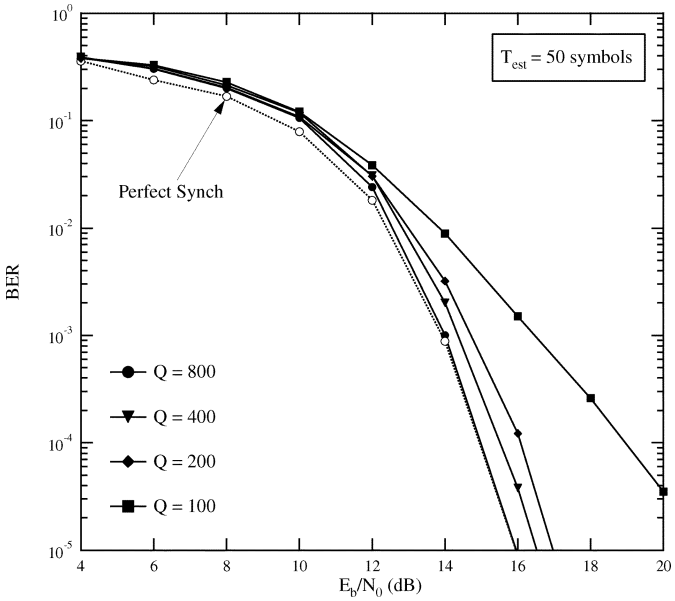

Fig. 9. BER versus E_b/N_0 for a differential receiver and a single user.

the ideal performance is achieved with $Q = 800$. Decreasing Q to 200 has modest consequences (a degradation of 1 dB), while a further decrease of Q to 100 entails a performance loss of about 5 dB at BER $= 10^{-5}$. The reduced sensitivity of the BER performance of the differential detector to the sampling rate comes from the fact that undersampling affects only the synchronization accuracy. There is no loss in signal energy since the decision statistic is computed by integrating the product $x(t)x(t - T_f)$ in analog form.

VI. Conclusion

Two data-aided timing recovery strategies based on LS methods have been investigated for applications in UWB communication systems. They operate on samples of the received waveform taken at a high rate on the order of one GHz. In addition to frame and symbol timing, they provide an estimate of the channel response, which is necessary in a coherent receiver. Their performance is comparable but their implementation complexity is different. The simplest scheme requires that the data transmission be interrupted at regular intervals and replaced by a periodic signal at frame rate. The other allows a continuous data transmission and does not need any channel access protocol.

Simulations have been run to assess the BER performance of coherent and differential receivers endowed with the proposed synchronization schemes. The BER degradations due to MAI have also been investigated and have been shown to be the result of two separate mechanisms: the growth of the interference at the detector input and the worsening of the synchronization and channel estimation functions. In general, the performance worsens as the sampling rate decreases as a consequence of the reduced signal energy in the samples. However, the effects are much larger in coherent rather than in differential receivers. In the former, halving the sampling rate entails a loss of 3 dB or more, depending on the number of users. In the latter, the degradation is more limited. With a single user, the loss is within 1 dB, even with sampling at 1/4 of the Nyquist rate.

Appendix

In this Appendix, we first show the explicit dependence of

$$D^2(\tilde{\nu},\tilde{\mu},\tilde{\mathbf{h}}) = \sum_{k=0}^{K-1}\sum_{m=0}^{N_f-1}\left\|\mathbf{x}_{k,m} - \mathbf{s}_{k,m}(\tilde{\mu},\tilde{\nu},\tilde{\mathbf{h}})\right\|^2 \tag{38}$$

on the components of $\tilde{\mathbf{h}}$, and then we minimize either $D^2(\tilde{\nu},\tilde{\mu},\tilde{\mathbf{h}})$ as a function of $\tilde{\nu}$ or $D^2(\tilde{\nu},\tilde{\mu},\tilde{\mathbf{h}})$ as a function of $(\tilde{\nu},\tilde{\mu},\tilde{\mathbf{h}})$. To begin, we expand the squared norm in (38), taking (24) into account. With the shorthand notations

$$\tilde{\mathbf{v}}_m^{(\downarrow)} = \mathbf{v}^{(\downarrow)}[\tilde{\mu} + N_c c_{|m-\tilde{\nu}|_{N_f}}, \tilde{\mathbf{h}}]$$
$$\tilde{\mathbf{v}}_{m-1}^{(\uparrow)} = \mathbf{v}^{(\uparrow)}[Q - \tilde{\mu} - N_c c_{|m-1-\tilde{\nu}|_{N_f}}, \tilde{\mathbf{h}}] \tag{39}$$
$$\tilde{a}_{k,m} = a_{k+\lfloor (m-\tilde{\nu})/N_f \rfloor}, \quad \tilde{a}_{k,m-1} = a_{k+\lfloor (m-1-\tilde{\nu})/N_f \rfloor} \tag{40}$$

we have

$$\begin{aligned}&\left\|\mathbf{x}_{k,m} - \mathbf{s}_{k,m}(\tilde{\mu},\tilde{\nu},\tilde{\mathbf{h}})\right\|^2 \\ &= \|\mathbf{x}_{k,m}\|^2 + \left\|\tilde{\mathbf{v}}_m^{(\downarrow)}\right\|^2 + \left\|\tilde{\mathbf{v}}_{m-1}^{(\uparrow)}\right\|^2 - 2\tilde{a}_{k,m}\mathbf{x}_{k,m}^T\mathbf{v}_m^{(\downarrow)} \\ &\quad -2\tilde{a}_{k,m-1}\mathbf{x}_{k,m}^T\tilde{\mathbf{v}}_{m-1}^{(\uparrow)} + 2\tilde{a}_{k,m}\tilde{a}_{k,m-1}(\tilde{\mathbf{v}}_m^{(\downarrow)})^T\tilde{\mathbf{v}}_{m-1}^{(\uparrow)}.\end{aligned} \tag{41}$$

Next, we observe that $(\tilde{\mathbf{v}}_m^{(\downarrow)})^T\tilde{\mathbf{v}}_{m-1}^{(\uparrow)} = 0$ since the interframe interference is negligible by assumption. Also, letting

$$u[l;a,b] \doteq \begin{cases} 1, & \text{for } a \le l \le b \\ 0, & \text{elsewhere} \end{cases} \tag{42}$$

it is easily checked that

$$\left\|\tilde{\mathbf{v}}_m^{(\downarrow)}\right\|^2 = \sum_{l=0}^{L-1}\tilde{h}^2[l]\,u[l;0,Q-\tilde{\mu}-N_c c_{|m-\tilde{\nu}|_{N_f}}-1] \tag{43}$$

$$\begin{aligned}\left\|\tilde{\mathbf{v}}_{m-1}^{(\uparrow)}\right\|^2 &= \sum_{l=0}^{L-1}\tilde{h}^2[l]\,u[l;Q-\tilde{\mu} \\ &\quad - N_c c_{|m-1-\tilde{\nu}|_{N_f}}, L-1]\end{aligned} \tag{44}$$

$$\begin{aligned}\mathbf{x}_{k,m}^T\tilde{\mathbf{v}}_m^{(\downarrow)} &= \sum_{l=0}^{L-1}\tilde{h}[l]\,x_{k,m}[l+\tilde{\mu}+N_c c_{|m-\tilde{\nu}|_{N_f}}] \\ &\quad \times u[l;0,Q-\tilde{\mu}-N_c c_{|m-\tilde{\nu}|_{N_f}}-1]\end{aligned} \tag{45}$$

$$\begin{aligned}\mathbf{x}_{k,m}^T\tilde{\mathbf{v}}_{m-1}^{(\uparrow)} &= \sum_{l=0}^{L-1}\tilde{h}[l]\,x_{k,m}[l+\tilde{\mu}+N_c c_{|m-1-\tilde{\nu}|_{N_f}}-Q] \\ &\quad \times u[l;Q-\tilde{\mu}-N_c c_{|m-1-\tilde{\nu}|_{N_f}},L-1].\end{aligned} \tag{46}$$

Substituting these results into (38) yields

$$\begin{aligned}D^2(\tilde{\nu},\tilde{\mu},\tilde{\mathbf{h}}) &= \sum_{k=0}^{K-1}\sum_{m=0}^{N_f-1}\|\tilde{\mathbf{x}}_{k,m}\|^2 \\ &\quad + \sum_{l=0}^{L-1}\tilde{h}^2[l]M[l;\tilde{\mu},\tilde{\nu}] \\ &\quad - 2\sum_{l=0}^{L-1}\tilde{h}[l]\sum_{k=0}^{K-1}\sum_{m=0}^{N_f-1}z_{k,m}[l;\tilde{\mu},\tilde{\nu}]\end{aligned} \tag{47}$$

where we have defined

$$\begin{aligned} z_{k,m}[l;\tilde{\mu},\tilde{\nu}] \doteq\, & a_{k+\lfloor (m-\nu)/N_f \rfloor} x_{k,m}[l+\tilde{\mu}+N_c c_{|m-\tilde{\nu}|_{N_f}}] \\ & u[l;0,Q-\tilde{\mu}-N_c c_{|m-\tilde{\nu}|_{N_f}}-1] \\ & + a_{k+\lfloor (m-1-\nu)/N_f \rfloor} \\ & \times x_{k,m}[l+\tilde{\mu}+N_c c_{|m-1-\tilde{\nu}|_{N_f}}-Q] \\ & u[l;Q-\tilde{\mu}-N_c c_{|m-1-\tilde{\nu}|_{N_f}}],L-1] \end{aligned} \tag{48}$$

$$\begin{aligned} M[l;\tilde{\mu},\tilde{\nu}] \doteq \sum_{k=0}^{K-1}\sum_{m=0}^{N_f-1} \Big[& u[l;0,Q-\tilde{\mu}-N_c c_{|m-\tilde{\nu}|_{N_f}}-1] \\ & + u[l;Q-\tilde{\mu}-N_c c_{|m-1-\tilde{\nu}|_{N_f}},L-1]\Big]. \end{aligned} \tag{49}$$

Suppose that $\tilde{\mu}$ and $\tilde{\mathbf{h}}$ are fixed, say, $\tilde{\mu}=\hat{\mu}$ and $\tilde{\mathbf{h}}=\hat{\mathbf{h}}$, and we want to minimize $D^2(\tilde{\nu},\tilde{\mu},\tilde{\mathbf{h}})$. From (47), we get

$$\begin{aligned} \hat{\nu} = \underset{0\le\tilde{\nu}\le N_f-1}{\arg\max} \Bigg\{ & \sum_{l=0}^{L-1} \hat{h}^2[l] M[l;\hat{\mu},\tilde{\nu}] \\ & -2\sum_{l=0}^{L-1}\hat{h}[l]\sum_{k=0}^{K-1}\sum_{m=0}^{N_f-1} z_{k,m}[l;\hat{\mu},\tilde{\nu}] \Bigg\}. \end{aligned} \tag{50}$$

Vice versa, suppose we want to minimize $D^2(\tilde{\nu},\tilde{\mu},\tilde{\mathbf{h}})$ as a function of $(\tilde{\nu},\tilde{\mu},\tilde{\mathbf{h}})$. Differentiating (47) with respect to the $\tilde{h}[l]$'s and setting the results to zero produces

$$\tilde{h}[l] = \frac{1}{M[l;\tilde{\mu},\tilde{\nu}]} \sum_{k=0}^{K-1}\sum_{m=0}^{N_f-1} z_{k,m}[l;\tilde{\mu},\tilde{\nu}], \quad 0\le l\le L-1. \tag{51}$$

Next, plugging this result into (47) gives

$$\begin{aligned} D^2(\tilde{\nu},\tilde{\mu},\tilde{\mathbf{h}}) = & \sum_{k=0}^{K-1}\sum_{m=0}^{N_f-1} \|x_{k,m}\|^2 \\ & - \sum_{l=0}^{L-1} \frac{1}{M[l;\tilde{\mu},\tilde{\nu}]} \left(\sum_{k=0}^{K-1}\sum_{m=0}^{N_f-1} z_{k,m}[l;\tilde{\mu},\tilde{\nu}] \right)^2 \end{aligned} \tag{52}$$

and minimizing with respect to $(\tilde{\mu},\tilde{\nu})$ leads to

$$(\hat{\mu},\hat{\nu}) = \underset{(\tilde{\mu},\tilde{\nu})}{\arg\max} \left\{ \sum_{l=0}^{L-1} \frac{1}{M[l;\tilde{\mu},\tilde{\nu}]} \left(\sum_{k=0}^{K-1}\sum_{m=0}^{N_f-1} z_{k,m}[l;\tilde{\mu},\tilde{\nu}] \right)^2 \right\}. \tag{53}$$

Finally, substituting into (51), we have

$$\hat{h}[l] = \frac{1}{M[l;\tilde{\mu},\tilde{\nu}]} \sum_{k=0}^{K-1}\sum_{m=0}^{N_f-1} z_{k,m}[l;\hat{\mu},\hat{\nu}], \quad 0\le l\le L-1. \tag{54}$$

REFERENCES

[1] "In the matter of revision of the Commission's rules regarding ultra-wideband transmission systems," Federal Commun. Commission, Washington, DC, 2002.

[2] M. Z. Win and R. A. Scholtz, "Ultra-wide bandwidth time-hopping spread-spectrum impulse radio for wireless multiple access communications," *IEEE Trans. Commun.*, vol. 48, no. 4, pp. 679–691, Apr. 2000.

[3] ——, "On the robustness of ultra-wide bandwidth signals in dense multipath environments," *IEEE Commun. Lett.*, vol. 2, no. 2, pp. 51–53, Feb. 2003.

[4] M. Z. Win, "Spectral density of random time-hopping spread-spectrum UWB signals," *IEEE Commun. Lett.*, vol. 6, no. 12, pp. 526–528, Dec. 2002.

[5] M. Z. Win and R. A. Scholtz, "Characterization of ultra-wide bandwidth wireless communications channels: A communication theoretic view," *IEEE J. Sel. Areas Commun.*, vol. 20, no. 12, pp. 1613–1627, Dec. 2002.

[6] R. J. Cramer, R. A. Scholtz, and M. Z. Win, "Evaluation of an ultra-wideband propagation channel," *IEEE Trans. Antennas Propag.*, vol. 50, no. 5, pp. 561–570, May 2002.

[7] M. Z. Win and R. A. Scholtz, "Impulse radio: How it works," *IEEE Commun. Lett.*, vol. 2, no. 2, pp. 36–38, Feb. 1998.

[8] D. Porcino and W. Hirt, "Ultra-wideband radio technology: Potential and challenge ahead," *IEEE Commun. Mag.*, vol. 31, no. 7, pp. 66–73, Jul. 2003.

[9] J. L. Lee and R. A. Scholtz, "Ranging in a dense multipath environment using an UWB radio link," *IEEE J. Sel. Areas Commun.*, vol. 20, no. 12, pp. 1677–1683, Dec. 2002.

[10] M. Z. Win and R. A. Scholtz, "On the energy capture of ultrawide bandwidth signals in dense multipath environments," *IEEE Commun. Lett.*, vol. 2, no. 9, pp. 245–247, Sep. 1998.

[11] V. Lottici, A. N. D'Andrea, and U. Mengali, "Channel estimation for ultra-wideband communications," *IEEE J. Sel. Areas Commun.*, vol. 20, no. 12, pp. 1638–1645, Dec. 2002.

[12] R. C. Qiu, "A study of the ultra-wideband wireless propagation channel and optimum UWB receiver design," *IEEE J. Sel. Areas Commun.*, vol. 20, no. 12, pp. 1628–1637, Dec. 2002.

[13] R. Qiu and I.-T. Lu, "Multipath resolving with frequency dependence for wideband channel modeling," *IEEE Trans. Veh. Technol.*, vol. 48, no. 1, pp. 273–285, Jan. 1999.

[14] Y.-L. Chao and R. Scholtz, "Optimal and suboptimal receivers for ultra-wideband transmitted reference systems," in *Proc. IEEE Globecom*, vol. 6, Dec. 2003, pp. 759–763.

[15] G. Durisi and S. Benedetto, "Performance of coherent and noncoherent receivers for UWB communications," in *Proc. IEEE Int. Conf. Commun.*, vol. 2, May 2004, pp. 3429–3433.

[16] S. Franz and U. Mitra, "On optimal data detection for UWB transmitted reference systems," in *Proc. IEEE Globecom*, vol. 2, Dec. 2003, pp. 744–748.

[17] R. Hoctor and H. Tomlinson, "Delay-hopped transmitted-reference RF communications," in *Proc. IEEE Conf. Ultra Wideband Syst. Technol.*, 2002, pp. 265–269.

[18] T. Q.-S. Quek and M. Z. Win, "Ultrawide bandwidth transmitted reference signaling," in *Proc. IEEE Int. Conf. Commun.*, vol. 6, Jun. 2004, pp. 3409–3413.

[19] J. D. Choi and W. E. Stark, "Performance of ultra-wideband communications with suboptimal receivers in multipath channels," *IEEE J. Sel. Areas Commun.*, vol. 20, no. 12, pp. 1754–1766, Dec. 2002.

[20] W. Suwansantisuk and M. Z. Win, "Fundamental limits on spread spectrum signal acquisition," in *Proc. Conf. Inf. Sci. Syst.*, Baltimore, MD, Mar. 2005, [CD-ROM].

[21] ——, "Optimal search procedures for spread spectrum acquisition," in *Proc. Conf. Inf. Sci. Syst.*, Baltimore, MD, Mar. 2005, [CD-ROM].

[22] S. Gezici, E. Fishler, H. Kobayashi, H. V. Poor, and A. F. Molisch, "A rapid acquisition technique for impulse radio," in *Proc. IEEE Pacific Rim Conf. Commun., Comput., Signal Process.*, vol. 2, Aug. 2003, pp. 627–630.

[23] W. M. Lovelace and J. K. Townsend, "The effects of timing jitter on the performance of impulse radio," *IEEE J. Sel. Areas Commun.*, vol. 20, no. 12, pp. 1646–1651, Dec. 2002.

[24] Z. Tian and G. B. Giannakis, "BER sensitivity to mistiming in correlation-based UWB receivers," in *Proc. IEEE Globecom*, vol. 2, Dec. 2003, pp. 441–445.

[25] E. A. Homier and R. A. Scholtz, "Rapid acquisition of ultra-wideband signals in the dense multipath channel," in *Proc. IEEE Conf. Ultra Wideband Syst. Technol.*, May 2002, pp. 245–250.

[26] R. Blazquez, P. Newaskar, and A. Chandrakasan, "Coarse acquisition for ultra-wideband digital receivers," in *Proc. Int. Conf. Acoust., Speech, Signal Process.*, vol. 4, Apr. 2003, pp. IV:137–140.

[27] E. A. Homier and R. A. Scholtz, "Hybrid fixed-dwell-time search techniques for rapid acquisition of ultra-wideband signals," in *Proc. IEEE Int. Workshop Ultra-Wideband Syst.*, Oulu, Finland, Jun. 2003, [CD-ROM].

[28] L. Yang, Z. Tian, and G. B. Giannakis, "Non-data aided timing acquisition of ultra-wideband transmissions using cyclostationarity," in *Proc. IEEE Int. Conf. Acoust., Speech, Signal Process.*, vol. 4, Apr. 2003, pp. 121–124.

[29] L. Yang and G. B. Giannakis, "Low-complexity training for rapid timing acquisition in ultra-wideband communications," in *Proc. IEEE Globecom*, vol. 2, Dec. 2003, pp. 769–773.

[30] Z. Tian and V. Lottici, "Efficient timing acquisition in dense multipath for UWB communications," in *Proc. IEEE Veh. Technol. Conf.*, Dec. 2003, pp. 1318–1322.

[31] I. Maravic and M. Vetterli, "Low-complexity subspace methods for channel estimation and synchronization in ultra-wideband systems," in *Proc. IEEE Int. Workshop Ultra Wideband Syst.*, Oulu, Finland, Nov. 2003, [CD-ROM].

[32] C. Carbonelli, U. Mengali, and U. Mitra, "Synchronization and channel estimation for UWB signals," in *Proc. IEEE Globecom*, vol. 2, Dec. 2003, pp. 764–768.

[33] C. Carbonelli and U. Mengali, "Timing recovery for UWB signals," in *Proc. IEEE Globecom*, vol. 1, Dec. 2004, pp. 61–65.

[34] "Channel Model Subcommittee Final Report," IEEE P802.15 Working Group for Wireless Personal Area Networks, 2002.

Cecilia Carbonelli (S'01–M'06) was born in Pisa, Italy, in 1976. She received the Laurea degree in telecommunications engineering and the Ph.D. degree in information engineering from the University of Pisa, Pisa, Italy, in 2001 and 2005, respectively.

During 2003, she was a Visiting Scholar with the Department of Electrical Engineering Systems, Communications Sciences Institute, University of Southern California, Los Angeles, where she is now a Postdoctoral Researcher. Her research interests include the area of digital communication theory, with special emphasis on third-generation code-division multiple-access systems, ultra-wideband communications, parameter estimation, and synchronization techniques.

Umberto Mengali (M'69–SM'85–F'90–LF'03) received the degree in electrical engineering from the University of Pisa, Pisa, Italy, in 1961.

In 1971, he received the Libera Docenza in Telecommunications from the Italian Education Ministry and in 1975 was made a Professor of electrical engineering with the Department of Information Engineering, University of Pisa. In 1994, he has been a Visiting Professor with the University of Canterbury, Christchurch, New Zealand, as an Erskine Fellow. His research interests are in the area of digital communications and communication theory, with emphasis on synchronization methods and modulation techniques. He has published over 90 journal papers and coauthored the book *Synchronization Techniques for Digital Receivers* (New York: Plenum, 1997).

Prof. Mengali has been an Editor for the IEEE TRANSACTIONS ON COMMUNICATIONS and of the *European Transactions on Telecommunications.* He is listed in *American Men and Women in Science.*